https://doi.org/10.5194/se-2020-145
Preprint. Discussion started: 16 September 2020

Solid Earth Discussions

Gravity Effect of Alpine Slab Segments Based on Geophysical and Petrological Modelling

Maximilian Lowe [1], Jörg Ebbing [1], Amr El-Sharkawy [1,2], Thomas Meier [1]

[1]Institute for Geosciences, Kiel University, Germany
[2]National Research Institute of Astronomy and Geophysics, 11421, Helwan, Cairo, Egypt
Correspondence to Maximilian Lowe: maximilian.lowe@gmx.de

Abstract

We study the potential gravity effect of suggested slab configurations beneath the Alpine mountain belt. The opposing slab configurations are based on seismic crustal thickness estimates and high-resolution upper mantle tomographies. Direct conversion of upper mantle seismic velocities to densities results in a gravity response that reflects results in a gravity field that may be interpreted as related to the effect of subducting lithosphere, however the different contributing slab segments cannot be clearly identified. Therefore, we define the geometry of the upper slab interface by using the crustal thickness at 40 km depth as upper starting point. Based on seismic tomography, the slab interface is followed down to 200 km depth. We define two alternative models for the slab configuration in the Alpine region in line with recently proposed hypotheses. The gravity effect of these alternative models is calculated for (i) a simple constant density distribution in the slab and (ii) accounting for compositional and thermal variations with depth. The forward calculations predict a gravity effect of the slab up to 40 mGal and significant differences in the pattern of the anomalies.

Keywords:
Satellite gravity gradient, Alpine subduction, lithospheric and sub lithospheric structure, mantle composition, seismic tomography

1. Introduction

The formation and present geodynamics of the Alps are linked to long lasting tectonic processes, including Adria-Europe continent-continent collision, subduction of oceanic and continental lithosphere, the formation of crustal nappes as well as extensional and compressional processes (Frisch, 1979; Stampfli & Borel, 2002; Handy, et al., 2010, 2015). A major role in the present geodynamics of the Alpine region plays the Adriatic (or Adria) microplate, which is trapped between the converging major plates of Europe and Africa. Adria is moving counter-clockwise with respect to Europe and is subducted beneath the Apennines to the west as well as to the east beneath the Dinarides, while colliding with Eurasia in the Alps to the north (e.g. Channel & Horvath, 1976; Dewey et al., 1989; Stampfli & Borel, 2002; Handy et al., 2010; Le Breton et al., 2017). Subducting slab segments have been imaged by different seismological body-wave travel-time tomographies as well as surface-wave tomographies

https://doi.org/10.5194/se-2020-145
Preprint. Discussion started: 16 September 2020

within the Alpine upper mantle (e.g., Lippitsch et al., 2003; Spakman & Wortel, 2004; Mitterbauer et al. 2011; Zhao et al., 2016; Kästle et al., 2018; El-Sharkawy et al., 2020). However, the configuration of subducting slab segments remains controversial. In the Western Alps, Lippitsch et al. (2003) propose a slab break-off, which is in line with the findings of Beller et al. (2018) and Kästle et al. (2018). Kästle et al. (2020) support the presence of a slab break-off at about 100 km depth. In contrast, a continuous subducting slab segment in the Western Alps, down to at least 250 km depth, is imaged by a number of other tomographic models (e.g. Koulakov et al., 2009; Zhao et al., 2016; Hua et al., 2017; Lyu et al., 2017).

A continuous subduction of Eurasia beneath the Central Alps down to at least 200 km depth has been imaged by different tomographic models (e.g. Lippitsch et al., 2003; Piromallo and Morello, 2003; Koulakov et al., 2009; Mitterbauer et al., 2011; Hua et al., 2017; Fichtner et al., 2018; El-Sharkawy et al., 2020). The slab configuration and subduction direction in the Eastern Alps remains unclear. According to the classical view, Eurasia is been subducted beneath Adria in a southward subduction (Hawkesworth et al., 1975; Lüschen et al., 2004; 2006). This idea was first challenged by Lippitsch et al. (2003), Schmid et al. (2004), Kissling et al. (2006) and Handy et al. (2015). Instead, they argued for slab break-off in the eastern Alps and a northward-dipping Adriatic slab in the easternmost Alps, leading to a switch of the slab polarity, as Adria is subducting beneath the European plate (Handy et al., 2015). The view that Adriatic and not Eurasian lithosphere is subducting northwards in the Eastern Alps has been opposed by Mitterbauer et al. (2011), as their model shows a northward dipping slab in the eastern most Alps connected to the European plate. Recently, subduction of both Eurasian and Adriatic lithosphere in the eastern Alps down to about 150 km has been proposed by Kästle et al. (2020) and El-Sharkawy et al. (2020). For a more in-depth discussion of tomographic Alpine models the reader is referred to Kästle et al. (2020).

https://doi.org/10.5194/se-2020-145
Preprint. Discussion started: 16 September 2020

Solid Earth Discussions

Previous models, which address the Alpine gravity field have not considered any slab segments, but only account for the thickness of the lithosphere (e.g. Ebbing et al., 2006; Spooner et al., 2019). In the Bouguer Anomaly of the Alps (Fig. 1a), no direct indication of subducting slabs is seen (in contrast to the Andes subcution zone) as the field is dominate by crustal thickness and intra-crustal sources (Ebbing et al., 2006). However, subducting slabs have a higher density than the ambient mantle, which should result in a positive gravity effect. In this study we aim at quantifying these contributions.

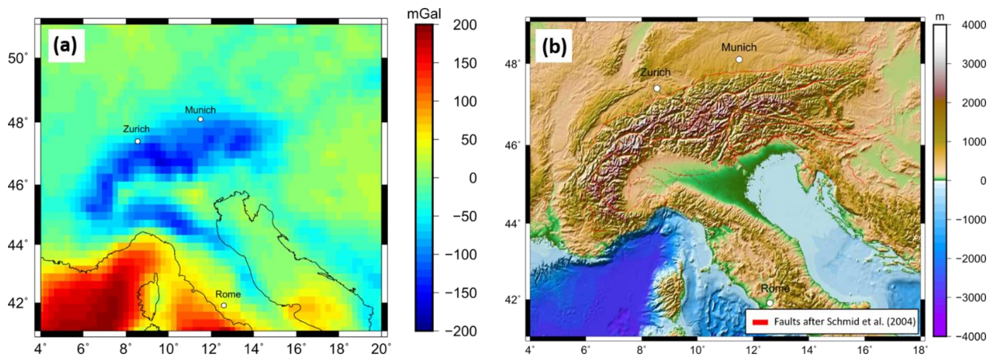

Figure. 1 ***(a)*** *Bouguer Anomaly based on XGM 2019 at a station height of 6040m, just above the surface of the Alps.* ***(b)*** *Topography from ETOPO 1 from Amante and Eakins (2009). Faults in red after Schmid et al. (2004).*

We present three different approaches to model the gravity effect of the slab segments and discuss the strength and limitations of the applied methods. Hereby, we convert seismic velocities to density. We also use seismic crustal thickness estimations and upper mantle tomographic models to define slab geometries and test two different slab configurations. Furthermore, we estimate the influence of composition on the density structure within the slab segment in order to quantify the expected gravity effect.

2. Data

The Bouguer Anomaly (Fig. 1a) is based on the global model *XGM 2019* (Zingerle et al., 2019) developed for spherical harmonics up to degree 719, with a resolution of ~25 km (half wavelength). The simple Bouguer Anomaly is calculated from the free-air gravity disturbance with a topographic density of 2670 kg/m^3, and water density of 1030 kg/m^3 for the offshore

https://doi.org/10.5194/se-2020-145
Preprint. Discussion started: 16 September 2020

areas. For the topography/bathymetry, we use ETOPO1 with a 1 arc minute resolution (Amante & Eakins, 2009). The gravity field is defined at a constant station height of 6040 m. The resulting Bouguer Anomaly shows a gravity low in the order of -200 mGal over the high topography of the Alps, indicating an isostatic compensation (e.g. Ebbing et al., 2006). Additionally, we calculated gravity gradients at a station height of 225 km representing the GOCE satellite altitude. The results of the gradient calculations can be found in the appendix.

For the definition of the slab geometry, we use crustal thickness estimates based on the receiver function study by Spada et al. (2013), supplemented by the Moho depth model of the European plate by Grad et al. (2009) in the surrounding and in areas not covered by Spada et al. (2013). For example, in the Eastern Alps the Moho depth model of Spada et al. (2013) shows a gap, interpreted as response to Alpine collisional processes. These areas and surroundings are filled with crustal depth estimation from Grad et al. (2009), both data sets were merged using a cosine taper with a taper width of 2°. The merged Moho depth map is sampled at a regular grid with a cell size of 0.25° (Fig. 2)

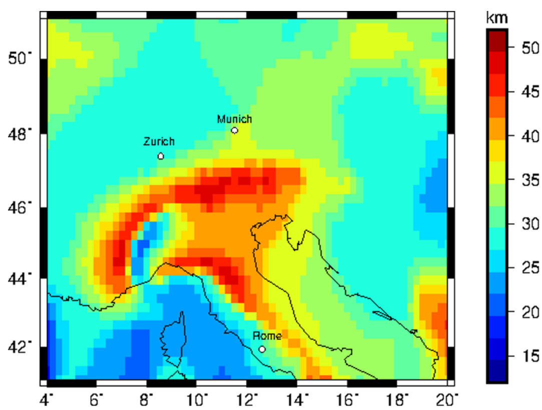

Figure 2 Merged crustal thickness map from Spada et al. (2016) and Grad et al. (2009) with a grid resolution of 0.25°.

For the upper mantle seismic velocity, the 3-D shear wave velocity model (MeRE2020) of (El-Sharkawy,2020) is used (Fig. 3). The model covers the upper mantle across the Alpine-Mediterranean area down to a depth of 300 km and absolute shear-wave velocities are given.

https://doi.org/10.5194/se-2020-145
Preprint. Discussion started: 16 September 2020

In this study, relative shear-wave velocities in the depth range from 70 to 200 km are calculated with respect to a depth-dependent average shear-wave velocity 1-D model. The upper limit of 70 km is introduced because we focus on the contribution of the slab segments removing therefore crustal information from the model. The lower boundary of 200 km is chosen based on clear images of the Central Alpine Slab to at least 200 km depth, as discussed in section 1, and the assumptions that depth larger than 200 km will have a negligible effect on the regional gravity field considered here.

The ambient noise tomography by Kästle et al. (2018) is used to define the geometry of the Western Alpine slab segment, hence we follow the idea of a slab-breakoff in the Western Alps at 100km depth (Kästle et al., 2020) as suggested also by Lippitsch et al. (2003) and Beller et al. (2018). For the eastern Alps, we consider two alternative models. For the first hypothesis, the P-wave tomography by Lippitsch et al. (2003) is used, to define the Eastern Alpine slab segment. The second hypothesis is based on Kästle et al. (2020) and El-Sharkawy et al. (2020). It assumes southward subduction of a short Eurasian Slab as well as northward subduction of a short Adriatic Slab in the eastern Alps. The slab configurations which are incorporated in the Alpine density models are discussed in greater detail in section 4.1.

3 Conversion of seismic velocities into density distribution

Relative seismic velocity variations are dependent on temperature and pressure. Densities in the subsurface are also temperature and pressure dependent. A conversion factor (ζ) can describe the relation between relative seismic velocities and relative densities. A range for conversion factors has been proposed in the literature for different rock types ranging from 0.1 to 0.45 (e.g. Isaac et al., 1989; Isaak, 1992; Karato, 1993; Kogan and McNutt, 1993; Vacher et al., 1998). The relative shear-wave velocity distribution in a 3D domain from the tomography model MeRE2020 from El-Sharkawy (2020) is converted using a constant conversion factor (ζ)

https://doi.org/10.5194/se-2020-145
Preprint. Discussion started: 16 September 2020

of 0.3 for the depth range from 70 km to 200 km. The converted relative density distribution varies between -240 and 350 kg/m^3. High correlations between the structural pattern in the converted density distribution and the relative seismic velocities are observed (Fig. 3). The converted 3D relative density distribution includes all heterogeneities in the Alpine lithosphere and not only structures of the potential slab segments to which the tomography is sensitive. The relative density model is transferred into tesseroids with a horizontal expansion of 0.2° and a vertical expansion of 3 km.

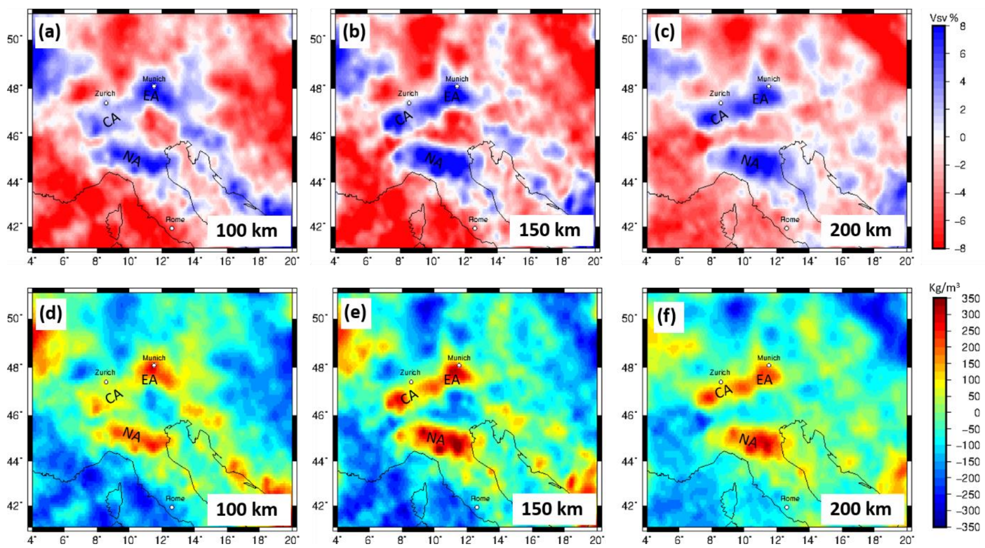

*Figure 3 **(a)-(c)** Depth slices of relative surface wave velocities (Vsv) from MeRE2020 (El-Sharkawy et al., 2020). **(d)-(f)** converted relative density distribution in different depths based on a conversion factor (ζ) of 0.3. CA = Central Alpine Slab; EA = Eastern Alpine Slab; NA = Northern Apennine Slab*

In the gravity field, a gravity high with a magnitude of ~40 mGal is observed over the Alps. That might be interpreted as relating to the proposed slab segments in the Northern Apennine and Alpine area. However, the graity field (and gradients, see appendix) is dominated by anomalies outside the Alpine realm (Fig. 4), for instance in the Ligurian Sea and the Dinaride-Hellenide Orogen.Therefore, in the next step, we try to concentrate on the seismic anomalies in the Alpine realm that can be related to the slab segments.

https://doi.org/10.5194/se-2020-145
Preprint. Discussion started: 16 September 2020

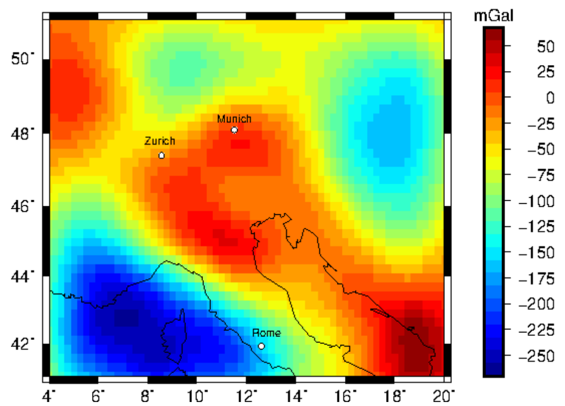

Figure 4 Forward calculated gravity signal from relative density distribution converted from relative seismic velocities using a conversion factor of 0.3.

4 Slab models

To estimate the gravity contribution of independent slab segments we introduce different models for the subducting lithosphere. In the first approach we use a set of models with simple constant density distribution in the slab, where the parameters, namely the density contrast and volume of the slab segment is varied. Secondly, we create a set of slab models accounting for compositional and thermal variations with depth. Those models are created with the software package LitMod 3D (Fullea et al., 2009) and will be referred as LitMod models in the following. For all non-LitMod models, the gravity and gravity gradients are calculated using tesseroids, which are spherical prisms (Uieda et al., 2016).

4.1 Alternative slab configurations

We define two alternative slab configurations based on a model of crustal thickness and different tomographic studies. Increasing crustal thickness is used as a direct indication for a subducting slab. The isoline for the slab front (upper boundary of the slab) geometries is here defined at the crustal mantle boundary at 44 km depth. At upper mantle depth, increased seismic velocity anomalies in tomographic models beneath the Alps are interpreted as contrast between colder and therefore denser subducting material to the ambient mantle material. At 100, 150,

https://doi.org/10.5194/se-2020-145
Preprint. Discussion started: 16 September 2020

and 200 km depth, the slab front isoline is defined at the 0% contour line of the relative seismic velocity, marking the transition from rocks with low velocity to high velocity rocks. The isolines at 44 km, 100 km, 150 km and 200 km depth are displayed upon the Alpine topography (Fig. 5 a-b) Vertical interpolation between the isolines of the slab front at different depths (40, 100, 150 and 200 km) result in a continuous slab front surface. The lower boundary of the slabs and therefore the thickness of the slab segment is not picked based on seismic data but assumed to have constant thicknesses for simplifications. The thickness is varied for different models from 60 to 100 km depth.

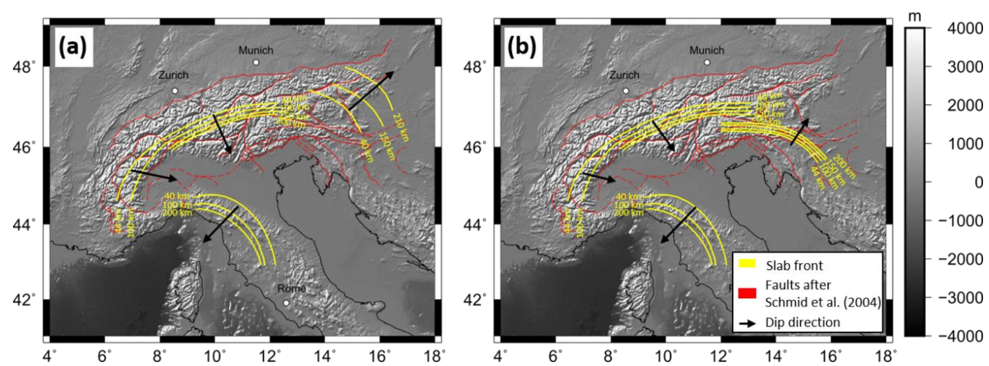

*Figure 5 Defined isolines based on crustal thickness estimations and seismological tomography models for the slab front for **(a)** Configuration 1 and **(b)** Configuration 2. Black arrows indicate the subduction direction. In red the fault configuration after Schmid et al. (2004).*

We define two different slab configurations. Configuration 1 (Fig. 5a) features a north subducting slab segment in the Eastern Alps based on Lippitsch et al. (2003). A Central Alpine slab segment is defined based on Lippitsch et al. (2003) and MeRE2020 (El-Sharkawy et al., 2020) subducting in southeast direction. The Eastern and Central Alpine slab segments are separated by a slab gap and show perpendicular subduction directions. The southeast-ward subducted slab segment in the Western Alps is defined using the tomographic model of Kästle et al. (2018), supporting the idea of slab break-off at about 100 km depth. In addition, a southwest-subducting slab segment beneath the northern Apennines is considered down to

https://doi.org/10.5194/se-2020-145
Preprint. Discussion started: 16 September 2020

about 200 km depth, as imaged by MeRE2020 (El-Sharkawy et al., 2020) because of its proximity to the western Alps.

Configuration 2 (Fig. 5b) considers a slab configuration mainly based on the interpretation of the MeRE2020 model (Fig. 3) by El-Sharkawy et al. (2020). In the Eastern Alps, both a short southward subducting Eurasian slab segment as well as a short northward subducting Adriatic slab are assumed. The Central and Western Alpine slab segments as well as the slab beneath the northern Apennines are identical to Configuration 1.

To estimate the gravity effect of the slab configurations, the geometries are discretized into tesseroids with a 0.2° extension in the horizontal domain and a vertical size of 20 km. The tesseroids range from 40 km to 220 km depth. First, a constant density contrast is assigned to the entire slab. We test density contrasts from 20 kg/m^3 to 80 kg/m^3. The thickness of the Alpine slab is not well constraint. We test for three slab volumes by assigning three slab thicknesses, 60 km, 80 km and 100 km based on studies on other subducting slab segments (e.g. Wang et al., 2020). Due to the curved geometries of the proposed slab segments rectangular tesseroids with a horizontal expansion of 0.2° will either over- or under-estimate the volume of a subducting slab at the edges of the slab. The percentage volume share of each tesseroid to the slab geometry is calculated. The assigned density of tesseroids which does not lay fully within the slab geometry is decreased according to the percentage volume within the slab geometry. Therefore, the density distribution correlates to the hypothetical slab positions and volumes in the Alpine subsurface without increasing the discretisation resolution of the tesseroid model beyond the uncertainty of gravity measurements and seismic tomographies.

Forward calculated slab models for predefined slab geometries of Configuration 1 and 2 with a constant density contrast of 60 kg/m^3 and a constant thickness of 80 km result in a sharp gravity signal ranging from 70 mGal to 100 mGal (Fig. 6). Both models generate a gravity signal in the order of magnitude of 70 mGal in the Central Alpine region as well as in the Apennine. The

https://doi.org/10.5194/se-2020-145
Preprint. Discussion started: 16 September 2020

Solid Earth Discussions
Open Access
EGU

gravity signal in the Eastern Alps differ for the two hypotheses (Fig. 6 a, b). The Western Alpine slab segment shows the weakest signal in both models.

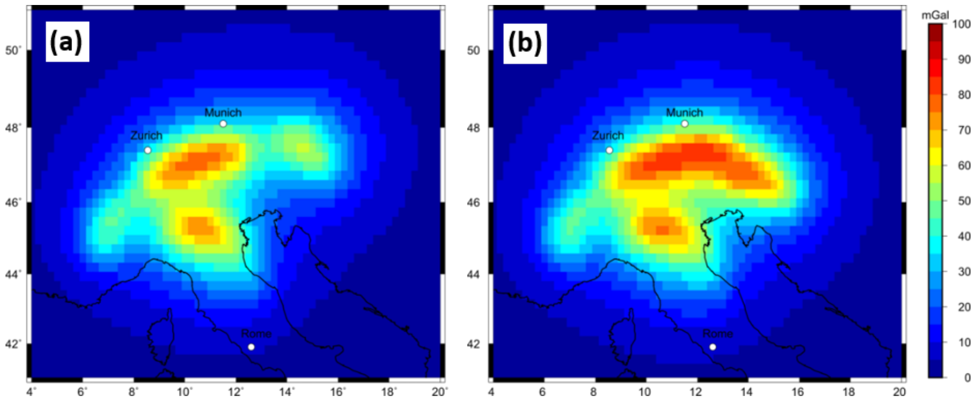

Figure 6 Forward calculated gz gravity signal at a station height of 6040 m from predefined slab geometries with a content density contrast of 60 kg/ m^3 and a constant thickness of 80 km. ***(a)*** *slab configuration of Configuration 1* ***(b)*** *slab configuration of Configuration 2.*

The gravity signal ranges from 30 to 110 mGal depending on the assigned density contrast and volume for both slab geometry models (Fig. 7). The highest magnitude of forward calculated gravity signal is in the order of 110 mGal and is observed for a slab model with a density contrast of 80 kg/m^3 and a constant slab volume of 100 km, while the lowest signal is produced by a combination of 20 km/m^3 density contrast and a slab thickness of 60 km. Similar gravity response is produced by different combinations of density contrast and volume. The signal pattern is influenced by the predefined slab geometry, while the magnitude of the gravity signal is depending on the density contrast and thickness (Fig. 7).

https://doi.org/10.5194/se-2020-145
Preprint. Discussion started: 16 September 2020

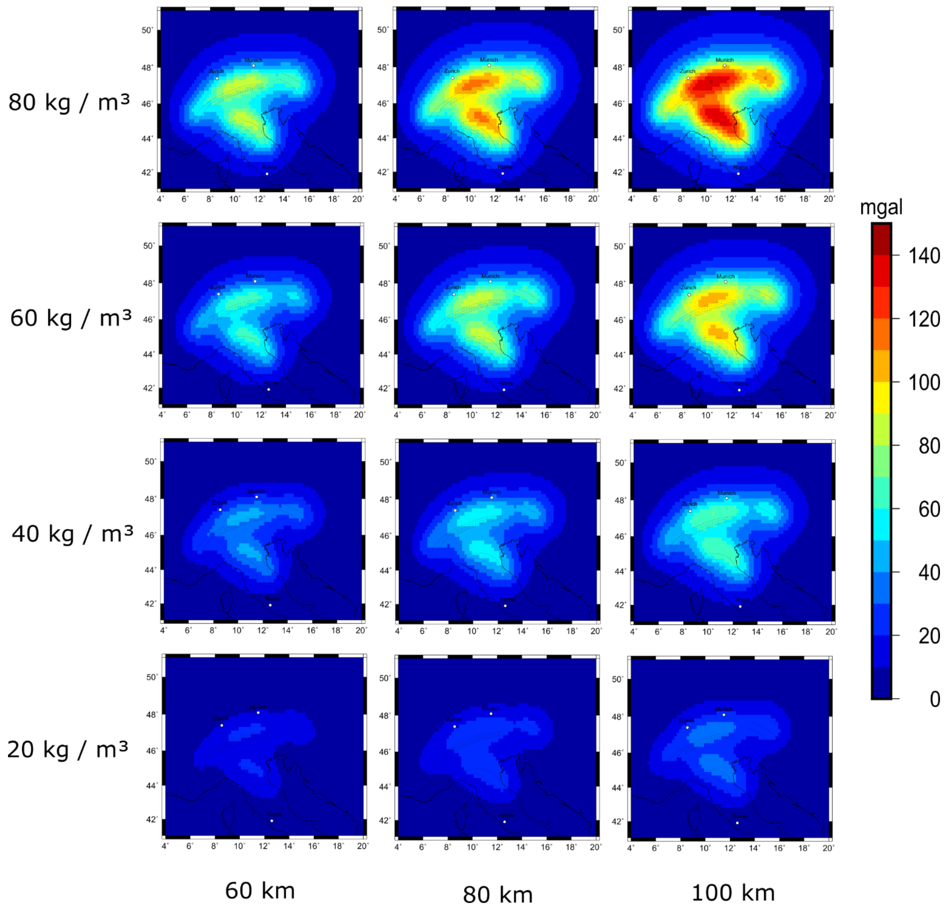

Figure 7 Forward calculated gz gravity signal for 12 different combination of density contrast and slab thickness at a station height of 6040 m.

Forward calculated gravity gradients at satellite height show the same dependency of signal strength (see Appendix).

4.2 Geophysical and petrological modelling with LitMod

For modelling the Alpine slab segments taking temperature and pressure variations as well as composition of the lithosphere and sub lithosphere into account, the geophysical and petrological modelling software LitMod 3D is utilized (Fullea et al.,2009). LitMod 3-D is a finite difference code, which allows the modelling of lithospheric and sub lithospheric structures down to 400 km depth by solving the heat transfer, thermodynamical, rheological, geopotential, and isostasy equations (Afonso et al., 2008; Fullea et al., 2010).

https://doi.org/10.5194/se-2020-145
Preprint. Discussion started: 16 September 2020

A LitMod model consists of a set of crustal, lithospheric- and sub lithospheric layers characterized by their petrophysical and thermal properties, which are used as input data (Fullea et al., 2010).

The assigned composition for the different layers is calculated using a LitMod subroutine which utilizes the perplex algorithm by Connolly (2009). Perplex calculates the specific bulk rock properties based on the six main lithospheric oxides (SiO_2, Al_2O_3, FeO, CaO, Na_2O) by minimizing Gibbs free energy equation. The Alpine lithosphere and sub lithosphere as well as the proposed slab segments are modelled using standard global lithospheric and sub lithospheric compositions to test the influence of compositional variations within the slab segments on the gravitational signal. Here, we use the so-called Tecton and Proterozoic type-composition (Table 1). Those compositions were chosen for a model with a homogene crust, lithosphere and sub lithosphere, where the density changes as a function of temperature and pressure based on the assigned compositions. The different slab composition is introduced to test whether a compositional contrast, in addition to the expected thermal difference, results in a significant density contrast between the slab and the ambient material.

Table 1: Mineralogical composition for the lithospheric and sub lithospheric structure.

Major Oxide Compositions	Aver. Tecton Gnt. SCLM [a]	Aver. Tecton Gnt. Peridotite [a]	Average Proterozoic Massif	PUM [b]	DMM [c]
SiO_2	44.5	45	45.2	45	44.7
Al_2O_3	3.5	3.9	2	4.5	3.98
FeO	8	8.1	7.9	8.1	8.1
MgO	39.8	38.7	41.6	37.8	37.8
CaO	3.1	3.2	1.9	3.6	3.17
Na_2O	0.26	0.24	0.13	0.36	0.13

[a] Classifications according to Griffin et al. (1999b), [b] McDonough & Sun (1995), [c] Workman & Hart (2005) DMM = Depleted mid-oceanic ridge basalt mantle, PUM = primitive upper mantle.

https://doi.org/10.5194/se-2020-145
Preprint. Discussion started: 16 September 2020

First, we create a reference model (M_0) without a slab segment. This model contains topography from the ETOPO1 dataset (Amante and Eakins, 2009), the merged Moho depths from Spada et al. (2013) and Grad et al. (2009). The lithosphere asthenosphere boundary (LAB) is a required interface for the LitMod 3D to divide the model between the lithosphere and sub lithosphere and to assign compositions. We set the LAB to a fix depth of 100 km depth throughout the model despite of the presence of slabs. In addition, we neglect the topography of the LAB for several reasons: i) the information of the lithospheric thickness in the Alpine forelands is spare and under constant discussion, ii) the fixed depth value is based on thermal isostasy LAB estimations from Artemieva et al. (2019), which shows a LAB depth in the range of 80 to 120 km depth in the Alpine forelands. This technical LAB is used to parameterize the model and is not meant to represent the topography of the LAB.

Slab segments are introduced stepwise for the lithosphere and sub lithosphere domains into the model as well as thermal anomalies for the sub lithospheric model part (Table 2). Calculating the difference to the reference model (M_0) allows to estimate the effect a slab segments has on the density, temperature distribution of the Alpine subsurface and therefore on the Alpine gravity field based on slab position, slab geometry and composition.

Table 2: Different LitMod models and there incorporated lithospheric and sub lithospheric structures and compositions.

Model	Composition
M_0	Lithosphere: aver. Tecton Gnt, sub lithosphere: PUM, no slab segment
M_1	Lithosphere: aver. Tecton Gnt, sub lithosphere: PUM, slab configuration: Configuration 1, lithospheric slab: Aver. Tecton Gnt. Peridotite, no sub lithospheric slab.
M_2	Lithosphere: aver. Tecton Gnt, sub lithosphere: PUM, slab configuration: Configuration 2, lithospheric slab: Aver. Tecton Gnt. Peridotite, no sub lithospheric slab.
M_3	Lithosphere: aver. Tecton Gnt, sub lithosphere: PUM, slab configuration: Configuration 1, lithospheric slab: Aver. Tecton Gnt. Peridotite, sub lithospheric slab: DMM, sub lithospheric temperature anomaly -100 °K
M_4	Lithosphere: aver. Tecton Gnt, sub lithosphere: PUM, slab configuration: Configuration 2, lithospheric slab: Aver. Tecton Gnt. Peridotite, sub lithospheric slab: DMM, sub lithospheric temperature anomaly -100 °K
M_5	Lithosphere: aver. Tecton Gnt, sub lithosphere: PUM, slab configuration: Configuration 1, lithospheric slab: Aver. Tecton Gnt. Peridotite, sub lithospheric slab: PUM, sub lithospheric temperature anomaly -100 °K

https://doi.org/10.5194/se-2020-145
Preprint. Discussion started: 16 September 2020

M_6	Lithosphere: aver. Tecton Gnt, sub lithosphere: PUM, slab configuration: Configuration 2, lithospheric slab: Aver. Tecton Gnt. Peridotite, sub lithospheric slab: PUM, sub lithospheric temperature anomaly -100 °K
M_7	Lithosphere: aver. Tecton Gnt, sub lithosphere: PUM, slab configuration: Configuration 1, lithospheric slab: Aver. Tecton Gnt. Peridotite, sub lithospheric slab: PUM, sub lithospheric temperature anomaly -200 °K
M_8	Lithosphere: aver. Tecton Gnt, sub lithosphere: PUM, slab configuration: Configuration 2, lithospheric slab: Aver. Tecton Gnt. Peridotite, sub lithospheric slab: PUM, sub lithospheric temperature anomaly -200 °K
M_9	Lithosphere: aver. Tecton Gnt, sub lithosphere: PUM, slab configuration: Configuration 2, lithospheric slab: Average Proterozoic Massif, no sub lithospheric slab

A positive density contrast between subducting material and the ambient mantle material results in a negative buoyancy force. A density contrast is introduced into the LitMod model by a difference in composition between the subducting denser slab and the surrounding mantle (Fig. 9). Here, we use Tecton like compositions for the lithosphere and the subducting slab segments since the Alpine slab segments result from continent-continent collision (Tables 1 and 2). A later model features a Proterozoic slab composition (M_9). Depleted mid-oceanic ridge basalt mantle (DMM) and primitive upper mantle (PUM) are used for the sub lithospheric domain. Additional to the density contrast within the sub lithosphere, a temperature anomaly of – 100 K is introduced for the sub lithospheric part. Later models include a variation of temperature anomalies (M_7, M_8). Note those compositions are used as a first order test and serve as a starting point for synthetic slab models to illustrate the compositional and thermal effect on the gravity signal by influencing the density distribution. They do not necessary represent the compositional mantle environment in the Alpine region.

https://doi.org/10.5194/se-2020-145
Preprint. Discussion started: 16 September 2020

Solid Earth Discussions
Open Access

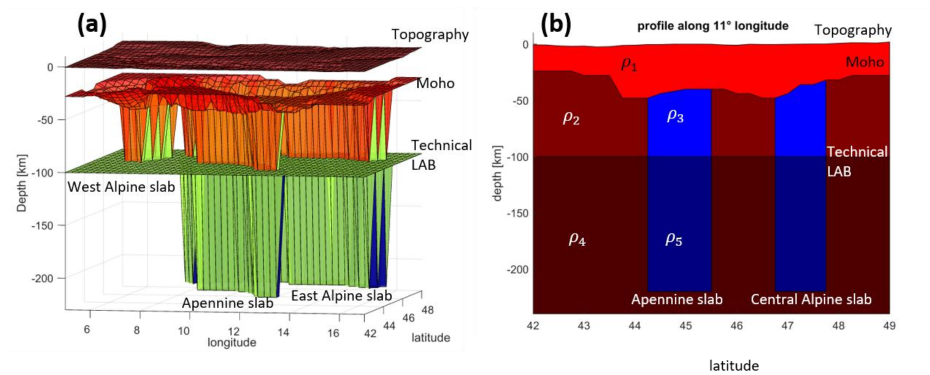

*Figure 8 **(a)** 3D model set up using LitMod 3D. Topography, Moho and LAB depth as well as the vertical incorporated slab models are used as input layers with assigned petrophysical and thermal properties. **(b)** Profile along 11° longitude through a LitMod model containing Topography, crustal and lithospheric thickness as well as a slab segment.* rho_{1-5} *indicate petrophysical and thermal property variations for each layer.*

A slab segment with an average Tecton Gnt. composition (M_1, M_2) results in a slightly denser material compared to the ambient mantle (M_0), while a slab segment with a Proterozoic composition (M_9) shows a less dense lithospheric structure compared to the reference model (M_0) (Fig. 10).

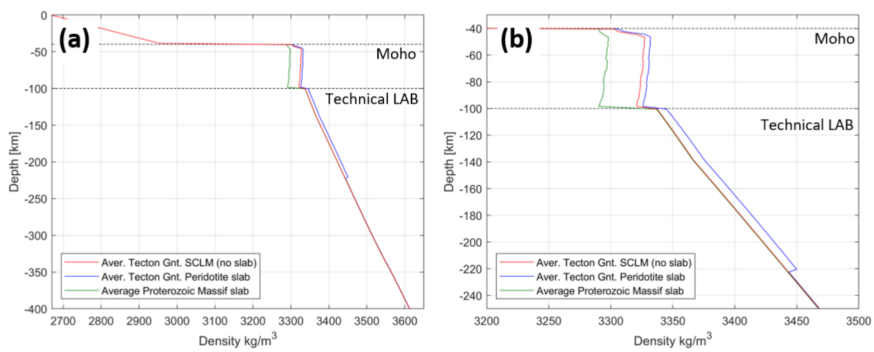

*Figure 9 **(a)** density profile at 11° longitude and 45° latitude for the full vertical model space of 400 km depth. Density profiles for 3 different models (M_0, M_1, M_9) with different compositional properties are shown. **(b)** Zoomed in profile at the depth range of present slab segments.*

The difference in density distribution (density contrast) within the slab segments with a Tecton composition (M_1, M_3) to the reference model (M_0) is in the order of 5 kg/m^3 for the lithosphere and in the order of 10 kg/m^3 for the sub lithospheric domain (Fig. 11). The density variations within the lithospheric and sub lithospheric domain are less than 1 kg/m^3. Between lithosphere and sub lithosphere, a rapid increase in density contrast is observed (Fig. 11A). The density

https://doi.org/10.5194/se-2020-145
Preprint. Discussion started: 16 September 2020

contrast of a lithospheric Proterozoic slab composition (M_9) to the reference model (M_0) is in the order of -30 kg/m^3 (Fig. 11b).

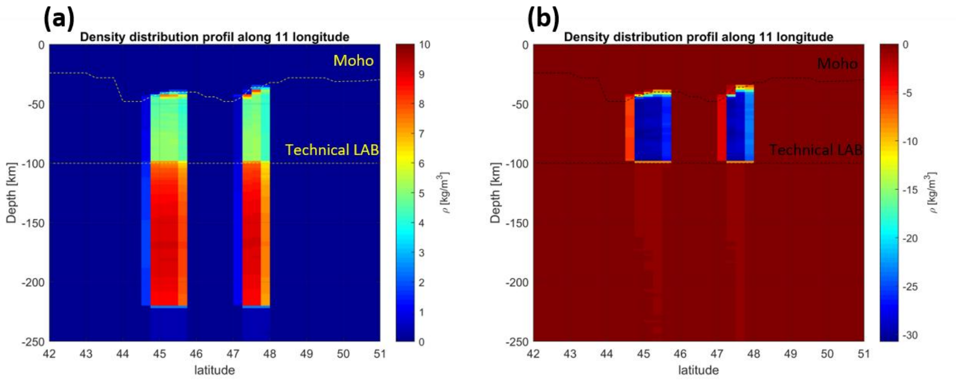

*Figure 10 **(a)** density contrast for lithospheric and sub lithospheric slab segments of model (M_3) with Tecton like composition within the lithosphere and PUM and DMM composition in the sub lithosphere with an additional thermal anomaly of -100° k for the sub lithospheric slab segment. **(b)** Lithospheric density contrast of a Proterozoic lithospheric slab segment to a Tecton compositional ambient mantle.*

The gravity signal caused by the proposed slab segment configurations is estimated for lithosphere and sub lithosphere separately. The forward calculated gravity effect, at surface height, for the slab configuration 1 for the lithospheric part is in the order of 4 mGal while the sub lithospheric gravity signal is in the range of 7 mGal (Fig. 12a, b). The combined gravity signal is in the order of 12 mGal (Fig. 12c). The gravity signal in the Eastern Alps for Configuration 2 is significant larger in the order of 17 mGal for the combined model (Fig. 12f).

https://doi.org/10.5194/se-2020-145
Preprint. Discussion started: 16 September 2020

Solid Earth
Discussions
Open Access

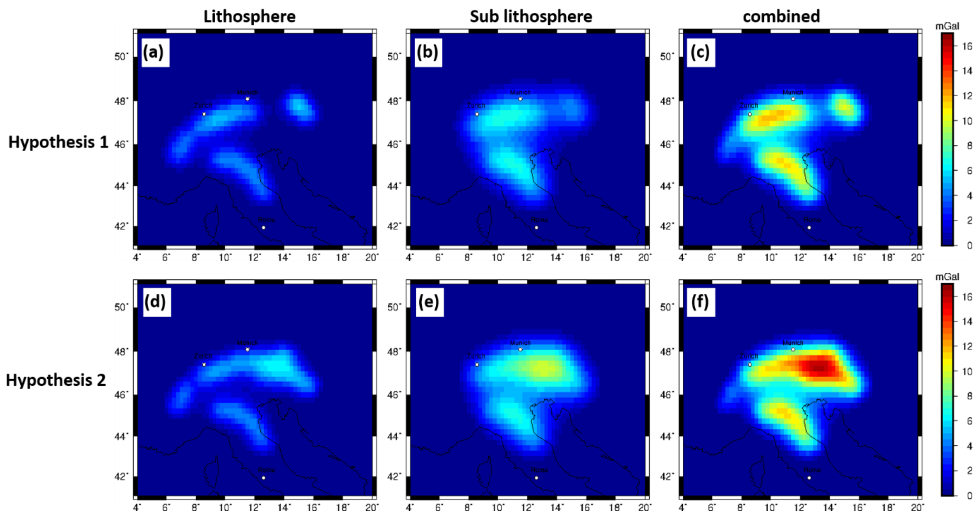

Figure 11 forward calculated gz gravity signal at surface station height based on LitMod models with Tecton like compositions in the lithosphere and PUM and DMM compositions in the sub lithosphere (M_1, M_2, M_3, M_4) with an additional thermal anomaly of -100° k for the sub lithospheric slab segment for predefined slab Configuration 1 ***(a)-(c)*** *and for Configuration 2* ***(d)-(f)****.*

The calculated gravitational effect of a slab segment with Proterozoic composition and a Tecton ambient mantle composition is in the order of 40 mGal for the gz component (Fig. 13 A).

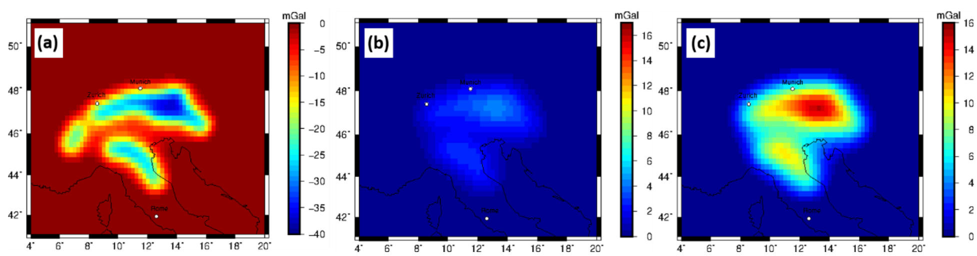

Figure 12 ***(a)*** *Forward calculated gravity effect of a Proterozoic lithospheric slab segment to a Tecton compositional ambient mantle for configuration.* ***(b)*** *gravity signal produced by purely compositional effect in the sub lithosphere between a PUM and DMM composition. for the gz component at station height. (c) gravity signal produced by purely thermal anomaly of -100° K for a sub lithospheric slab segment for the gz component at station height*

The gravity response to a compositional variation within the sub lithosphere between the incorporated slab segment (DMM composition) and the ambient mantle (PUM composition) is in the order of 4 mGal (Fig. 1b). The gravity response for a pure thermal anomaly of -100°K within the sub lithospheric slab segment is in the order of 16 mGal (Fig. 13c).

5 Discussion

The imprint of the gravity response within the gravity field caused by the density distribution based on direct conversion of seismic velocities is visible, however, individual and independent slab segments cannot be identified (Fig. 4). The strength of this approach is that it is fast to implement and can provide a first order characterization of the gravity signal and slab geometries of subducting lithosphere. However, a clear characterization of subducting slab segments is not possible. First of all, the density model depends on the resolution and regularization of the seismological model, which can lead to distortions in the gravity response (e.g. Root, 2020). The method is dependent on the choice of the conversion factor and might overestimate the density (see the large negative anomaly in the Ligurian Sea). For such a geodynamic complex area, a constant conversion factor is not adequate.

The forward calculated gravity field with competing predefined slab geometries shows a clear gravity signal, where the individual slab segments are distinguishable (Fig. 6).

A relative gravity low related to the slab gap in the Eastern Alps is a prominent feature in the gravity signal of Configuration 1 (Fig. 6a). The eastern Alpine slab segment of Configuration 1, due to its relatively small volume, result in a lower signal compared to the Central Alpine slab segment.

Configuration 2 shows a larger gravity signal in the Eastern Alps up to 100 mGal (Fig. 6b) compared to Configuration 1. The increase of the gravity signal is attributed to the subduction of both Eurasian and Adriatic lithosphere in the Eastern Alps. The gravity signal shows a continuous transition from the Central Alps to the Eastern Alps, where the contribution of the destined slab segment cannot be distinguished in the resulting gravity field (Fig. 6b). In the Western Alps, Configuration 1 and 2 show a lower gravity signal compared to the Central Alps. This is attributed to the much shallower Western Alpine slab segment reaching only a depth of 100 km.

The gravity signal depends both on the assigned density contrast and volume of the slab segment, both parameters affect the gravity signal, that the same gravity signal can be achieved

https://doi.org/10.5194/se-2020-145
Preprint. Discussion started: 16 September 2020

with different values of the density contrast and thickness, as gravity modelling is a non-unique solution (Fig. 7).

The calculated densities in LitMod 3-D models are estimated taking temperature and pressure variations into account based on an assigned composition. The composition has a strong influence on the resulting density contrast. In case, the compositional contrast between slab segment and ambient mantle is small, the density contrast is consequently small (Fig. 9 and 10a). With increasing differences in composition, the density contrast increases as well. A strong density contrast within the slab segment is recognizable between lithospheric and sub lithospheric domain (Fig. 10a and b), while the variations between the slab and ambient mantel remain small.

The gravity signal shows in the Eastern Alps significant larger signal from the lithosphere and sub lithosphere domain for Configuration 2 (Fig. 11d, e, and f) compared to Configuration 1 (Fig. 1a- c). The different slab segments are distinguishable with the exception of the two slab segments in the Eastern Alps in Configuration 2 (Fig. 11). The contribution from the the lithospheric domain to the gravity signal is smaller than from the sub lithospheric domain (Fig. 11b, and e). However, the slab gap and the eastern slab segment feature can be recognized in the lithospheric part in Configuration 1 but not in the gravity signal of the full model.

The Proterozoic slab segment has a larger gravity response compared to the Tecton-like composition. This gravitational signal is negative due to the less dense Proterozoic composition in comparison to the reference model (M_0) (Fig. 12a).

Sub lithospheric composition has only a small influence on the gravity field, in the order of less than 4 mGal (Fig. 12b and c). However, a thermal anomaly within the sub lithospheric slab in the order of -100 K result in a gravitational response of 16 mGal.

For all three modelling approaches (section 3) a measurable gravity effect of the subducting slab segments is seen. The independent slab segments are distinguishable to a certain degree with the exception of the bivergent slab configuration in the Eastern Alps (Fig. 4, 6, and 11),

https://doi.org/10.5194/se-2020-145
Preprint. Discussion started: 16 September 2020

while the slab configurations cannot be separated at satellite altitude (Appendix). Forward calculated gravity anomalies from converted density distribution suggest a gravitational signal of the slab segments in the order of 40 mGal which corresponds to a density contrast of 20 to 40 kg/m^3 in the models with predefined slab geometry. The models with a Tecton like composition suggest a gravity effect of the slab segments in the order of only 16 mGal, corresponding to a density contrast of 20 kg/m^3 in the simple model. Increasing the compositional difference with a Tecton composition suggests a gravity signal in order of 30 mGal and is in line with the converted density model.

All three methods show a slab contribution up to 40 mGal to the Alpine gravity field. That is significant in comparison to the observed Bouguer Anomaly with a minimum of ~200 mGal. If the slab contribution is not considered, a significant part of the gravity field is attributed to crustal thickness or intra-crustal sources. Due to the long-wavelength appearance of the gravity effect, that might not be relevant for small-scale or local studies, where the effect is only seen as a shift. For gravity models of larger areas (e.g. Eastern Alps) or even the entire regions that should not be neglected. For one, estimates of crustal thickness or the mass distribution are significantly biased, and placing the Alps in the geodynamic context of the surrounding requires a careful and complete consideration of all sources in order to provide realistic density distribution required for geodynamic models (e.g. Reuber et al., 2019).

6 Conclusions

We have addressed the potential gravity effect of proposed slab segments in the Alpine region using different modelling approaches.

- Converted density from seismic tomography: In the resulting gravity signal the imprint of slab segments is visible, however, distinguishing between the different and independent slab segments is not possible.

https://doi.org/10.5194/se-2020-145
Preprint. Discussion started: 16 September 2020

- Models with predefined slab segments are dependent on the assigned density contrast and volume as well as on the predefined positions of the slab segments. The gravity signal caused by the slab segments are sharp and can be separated for the different slab segments for the gravity field at the surface. Significant gravity contributions from slab segments below 200 – 250 km to the Alpine gravity are unlikely.

Combined petrophysical-geophysical modelling results in the most complex models. The calculated density variation within the slab is rather small compared to the density contrast between lithosphere and sub lithosphere. The density distribution within the slabs, and consequently the gravity field, is highly influenced by the slab composition.

All three modelling approaches suggest a positive gravitational effect of the Alpine slab segments up to 40 mGal. This is small, but significant compared to the -200 mGal in the observed Bouguer Anomaly. Previous studies compensated this effect by lithosphere thickness and/or intra-crustal sources, future studies should incorporate the structures in order to provide a meaningful representation of the geodynamic complex Alpine area, and with the integration of further observables might be able to judge on the correct slab configuration beneath the Alps.

Competing interests

The authors declare that they have no conflict of interest.

Author contributions

ML carried out the gravity modelling, visualized and interpreted the results and prepared the first manuscript draft. JE supervised the gravity modelling and interpretation, designed the original research project, acquisition of the financial support for the project leading to this publication and writing (reviewing and editing). TM defined the slab configurations based on

https://doi.org/10.5194/se-2020-145
Preprint. Discussion started: 16 September 2020

Solid Earth Discussions

tectonic and seismological knowledge and writing (reviewing and editing). AE created and provided the surface wave tomography model MeRE2020 and writing (reviewing and editing).

Acknowledgment

This study is part of the projects "Integrierte 3D Modellierung des Schwere- und Temperaturfelds zum Verständnis von Rheologie und Deformation der Alpen und ihrer Vorlandbecken - INTEGRATE" and "Surface Wavefield Tomography of the Alpine Region to Constrain Slab Geometries, Lithospheric Deformation and Asthenospheric Flow in the Alpine Region" funded by German Research Foundation (DFG) in the SPP Mountain Building Processes in 4D.

We thank the developer of open scientific Software which were utilized in this study: tesseroids (Uieda et al., 2016), LitMod 3D (Fullea et al., 2009 and Afonso et al., 2008) and Generic Mapping Tools (GMT) (Wessel & Luis, 2017).

References

Afonso, J. C., Fernandez, M., Ranalli, G., Griffin, W. L., & Connolly, J. A. D. (2008). Integrated geophysical-petrological modeling of the lithosphere and sublithospheric upper mantle: Methodology and applications. Geochemistry, Geophysics, Geosystems, 9(5).

Amante, C., & Eakins, B. W. (2009). ETOPO1 arc-minute global relief model: procedures, data sources and analysis.

Artemieva, I. M. (2019). Lithosphere structure in Europe from thermal isostasy. Earth-Science Reviews, 188, 454-468.

Beller, S., Monteiller, V., Operto, S., Nolet, G., Paul, A., & Zhao, L. (2018). Lithospheric architecture of the South-Western Alps revealed by multiparameter teleseismic full-waveform inversion. Geophysical Journal International, 212(2), 1369-1388.

Bouman, J., Ebbing, J., Fuchs, M., Sebera, J., Lieb, V., Szwillus, W., ... & Novak, P. (2016). Satellite gravity gradient grids for geophysics. Scientific reports, 6(1), 1-11.

Channell, J. E. T., & Horvath, F. (1976). The African/Adriatic promontory as a palaeogeographical premise for Alpine orogeny and plate movements in the Carpatho-Balkan region. Tectonophysics, 35(1-3), 71-101.

https://doi.org/10.5194/se-2020-145
Preprint. Discussion started: 16 September 2020

Connolly, J. A. D. (2009). The geodynamic equation of state: what and how. Geochemistry, Geophysics, Geosystems, 10(10).

Dewey, J. F., Helman, M. L., Knott, S. D., Turco, E., & Hutton, D. H. W. (1989). Kinematics of the western Mediterranean. Geological Society, London, Special Publications, 45(1), 265-283.

Ebbing, J., Braitenberg, C., & Götze, H. J. (2006). The lithospheric density structure of the Eastern Alps. Tectonophysics, 414(1-4), 145-155.

El-Sharkawy, A., Meier, T., Lebedev, S., Behrmann, J., Hamada, M., Cristiano, L., ... & Köhn, D. (2020). The Slab Puzzle of the Alpine-Mediterranean Region: Insights from a new, High-Resolution, Shear-Wave Velocity Model of the Upper Mantle. Geochemistry, Geophysics, Geosystems, e2020GC008993.

Fichtner, A., van Herwaarden, D. P., Afanasiev, M., Simutė, S., Krischer, L., Çubuk-Sabuncu, Y., ... & Trampert, J. (2018). The collaborative seismic earth model: Generation 1. Geophysical research letters, 45(9), 4007-4016.

Frisch, W. (1979). Tectonic progradation and plate tectonic evolution of the Alps. Tectonophysics, 60(3-4), 121-139.

Fullea, J., Afonso, J. C., Connolly, J. A. D., Fernandez, M., García-Castellanos, D., & Zeyen, H. (2009). LitMod3D: An interactive 3-D software to model the thermal, compositional, density, seismological, and rheological structure of the lithosphere and sublithospheric upper mantle. Geochemistry, Geophysics, Geosystems, 10(8).

Fullea, J., Fernàndez, M., Afonso, J. C., Vergés, J., & Zeyen, H. (2010). The structure and evolution of the lithosphere–asthenosphere boundary beneath the Atlantic–Mediterranean Transition Region. Lithos, 120(1-2), 74-95.

Grad, M., Tiira, T., & ESC Working Group. (2009). The Moho depth map of the European Plate. Geophysical Journal International, 176(1), 279-292.

Griffin, W. L., O'reilly, S. Y., Afonso, J. C., & Begg, G. C. (2009). The composition and evolution of lithospheric mantle: a re-evaluation and its tectonic implications. Journal of Petrology, 50(7), 1185-1204.

Handy, M. R., Schmid, S. M., Bousquet, R., Kissling, E., & Bernoulli, D. (2010). Reconciling plate-tectonic reconstructions of Alpine Tethys with the geological–geophysical record of spreading and subduction in the Alps. Earth-Science Reviews, 102(3-4), 121-158.

Handy, M. R., Ustaszewski, K., & Kissling, E. (2015). Reconstructing the Alps–Carpathians–Dinarides as a key to understanding switches in subduction polarity, slab gaps and surface motion. International Journal of Earth Sciences, 104(1), 1-26.

Hawkesworth, C. J., Waters, D. J., & Bickle, M. J. (1975). Plate tectonics in the Eastern Alps. Earth and Planetary Science Letters, 24(3), 405-413.

Hua, Y., Zhao, D., & Xu, Y. (2017). P wave anisotropic tomography of the Alps. Journal of Geophysical Research: Solid Earth, 122(6), 4509-4528.

https://doi.org/10.5194/se-2020-145
Preprint. Discussion started: 16 September 2020

Isaak, D. G., Anderson, O. L., Goto, T., & Suzuki, I. (1989). Elasticity of single-crystal forsterite measured to 1700 K. Journal of Geophysical Research: Solid Earth, 94(B5), 5895-5906.

Isaak, D. G. (1992). High-temperature elasticity of iron-bearing olivines. Journal of Geophysical Research: Solid Earth, 97(B2), 1871-1885.

Karato, S. I. (1993). Importance of anelasticity in the interpretation of seismic tomography. Geophysical Research Letters, 20(15), 1623-1626.

Kästle, E. D., El-Sharkawy, A., Boschi, L., Meier, T., Rosenberg, C., Bellahsen, N., ... & Weidle, C. (2018). Surface wave tomography of the alps using ambient-noise and earthquake phase velocity measurements. Journal of Geophysical Research: Solid Earth, 123(2), 1770-1792.

Kästle, E. D., Rosenberg, C., Boschi, L., Bellahsen, N., Meier, T., & El-Sharkawy, A. (2020). Slab break-offs in the Alpine subduction zone. International Journal of Earth Sciences, 1-17.

Kissling, E., Schmid, S. M., Lippitsch, R., Ansorge, J., & Fügenschuh, B. (2006). Lithosphere structure and tectonic evolution of the Alpine arc: new evidence from high-resolution teleseismic tomography. Geological Society, London, Memoirs, 32(1), 129-145.

Kogan, M. G., & McNutt, M. K. (1993). Gravity field over northern Eurasia and variations in the strength of the upper mantle. Science, 259(5094), 473-479.

Koulakov, I., Kaban, M. K., Tesauro, M., & Cloetingh, S. A. P. L. (2009). P-and S-velocity anomalies in the upper mantle beneath Europe from tomographic inversion of ISC data. Geophysical Journal International, 179(1), 345-366.

Le Breton, E., Handy, M. R., Molli, G., & Ustaszewski, K. (2017). Post-20 Ma motion of the Adriatic Plate: New constraints from surrounding orogens and implications for crust-mantle decoupling. Tectonics, 36(12), 3135-3154.

Lippitsch, R., Kissling, E., & Ansorge, J. (2003). Upper mantle structure beneath the Alpine orogen from high-resolution teleseismic tomography. Journal of Geophysical Research: Solid Earth, 108(B8).

Lüschen, E., Lammerer, B., Gebrande, H., Millahn, K., Nicolich, R., & TRANSALP Working Group. (2004). Orogenic structure of the Eastern Alps, Europe, from TRANSALP deep seismic reflection profiling. Tectonophysics, 388(1-4), 85-102.

Lüschen, E., Borrini, D., Gebrande, H., Lammerer, B., Millahn, K., Neubauer, F., ... & TRANSALP Working Group. (2006). TRANSALP—deep crustal Vibroseis and explosive seismic profiling in the Eastern Alps. Tectonophysics, 414(1-4), 9-38.

Lyu, C., Pedersen, H. A., Paul, A., Zhao, L., & Solarino, S. (2017). Shear wave velocities in the upper mantle of the Western Alps: new constraints using array analysis of seismic surface waves. Geophysical Journal International, 210(1), 321-331.

McDonough, W. F., & Sun, S. S. (1995). The composition of the Earth. Chemical geology, 120(3-4), 223-253.

Mitterbauer, U., Behm, M., Brückl, E., Lippitsch, R., Guterch, A., Keller, G. R., ... & Šumanovac, F. (2011). Shape and origin of the East-Alpine slab constrained by the ALPASS teleseismic model. Tectonophysics, 510(1-2), 195-206.

Piromallo, C., & Morelli, A. (2003). P wave tomography of the mantle under the Alpine‐Mediterranean area. Journal of Geophysical Research: Solid Earth, 108(B2).

Reuber, G., Meier, T., Ebbing, J., El-Sharkawy, A., & Kaus, B. (2019, January). Constraining the dynamics of the present-day Alps with 3D geodynamic inverse models-model version 0.2. In Geophysical Research Abstracts (Vol. 21).

Root, B. C. (2020). Comparing global tomography-derived and gravity-based upper mantle density models. Geophysical Journal International, 221(3), 1542-1554.

Schmid, S. M., Fügenschuh, B., Kissling, E., & Schuster, R. (2004). Tectonic map and overall architecture of the Alpine orogen. Eclogae Geologicae Helvetiae, 97(1), 93-117.

Spada, M., Bianchi, I., Kissling, E., Agostinetti, N. P., & Wiemer, S. (2013). Combining controlled-source seismology and receiver function information to derive 3-D Moho topography for Italy. Geophysical Journal International, 194(2), 1050-1068.

Spakman, W., & Wortel, R. (2004). A tomographic view on western Mediterranean geodynamics. In The TRANSMED atlas. The Mediterranean region from crust to mantle (pp. 31-52). Springer, Berlin, Heidelberg.

Spooner, C., Scheck-Wenderoth, M., Götze, H. J., Ebbing, J., & Hetényi, G. (2019). Density distribution across the Alpine lithosphere constrained by 3-D gravity modelling and relation to seismicity and deformation. Solid Earth, 10(6), 2073-2088.

Stampfli, G. M., & Borel, G. D. (2002). A plate tectonic model for the Paleozoic and Mesozoic constrained by dynamic plate boundaries and restored synthetic oceanic isochrons. Earth and Planetary Science Letters, 196(1-2), 17-33.

Uieda, L., Barbosa, V. C., & Braitenberg, C. (2016). tesseroids: Forward-modeling gravitational fields in spherical coordinates. Geophysics, 81(5), F41-F48.

Vacher, P., Mocquet, A., & Sotin, C. (1998). Computation of seismic profiles from mineral physics: the importance of the non-olivine components for explaining the 660 km depth discontinuity. Physics of the Earth and Planetary Interiors, 106(3-4), 275-298.

Wang, Y., He, Y., Lu, G., & Wen, L. (2020). Seismic, thermal and compositional structures of the stagnant slab in the mantle transition zone beneath southeastern China. Tectonophysics, 775, 228208.

Wessel, P., & Luis, J. F. (2017). The GMT/MATLAB Toolbox. Geochemistry, Geophysics, Geosystems, 18(2), 811-823.

Workman, R. K., & Hart, S. R. (2005). Major and trace element composition of the depleted MORB mantle (DMM). Earth and Planetary Science Letters, 231(1-2), 53-72.

https://doi.org/10.5194/se-2020-145
Preprint. Discussion started: 16 September 2020

Zhao, L., Paul, A., Malusà, M. G., Xu, X., Zheng, T., Solarino, S., ... & Aubert, C. (2016). Continuity of the Alpine slab unraveled by high-resolution P wave tomography. Journal of Geophysical Research: Solid Earth, 121(12), 8720-8737.

Zingerle, P., Pail, R., Gruber, T., & Oikonomidou, X. (2019). The experimental gravity field model XGM2019e.

Appendix A Gravity Gradients at satellite height

For all Alpine density models presented above we have calculated in addition to the gravity field (gz component) gravity gradients as well at a station height of 225 km. This height corresponds to the second mission phase of GOCE (Gravity field and steady-state ocean circulation explorer) carried out by ESA (European Space Agency). In contrast to gravity field (gz component) the different slab segments in the Alpine region are not distinguishable in the gravity gradient at satellite height. The longwave length signal of the different present slab segments contributes to a large-scale gravity response where the different contributor cannot be separated. We show the gravity gradients (mainly the gzz component) for completeness.

Measured gravity gradients from the GOCE mission (Bouman et al., 2016), which were corrected for topography and bathymetry ranges from 2.5 to -2.5 E at satellite altitude of 225 km height (Fig. 13). A negative gravity anomaly of -2.5 E in the gzz component is observed equivalent to the vertical gz component (Fig. 13). However, no clear sign for subducting lithosphere can be observed in any component of the gravity gradient tensor.

https://doi.org/10.5194/se-2020-145
Preprint. Discussion started: 16 September 2020

Solid Earth
Discussions
Open Access

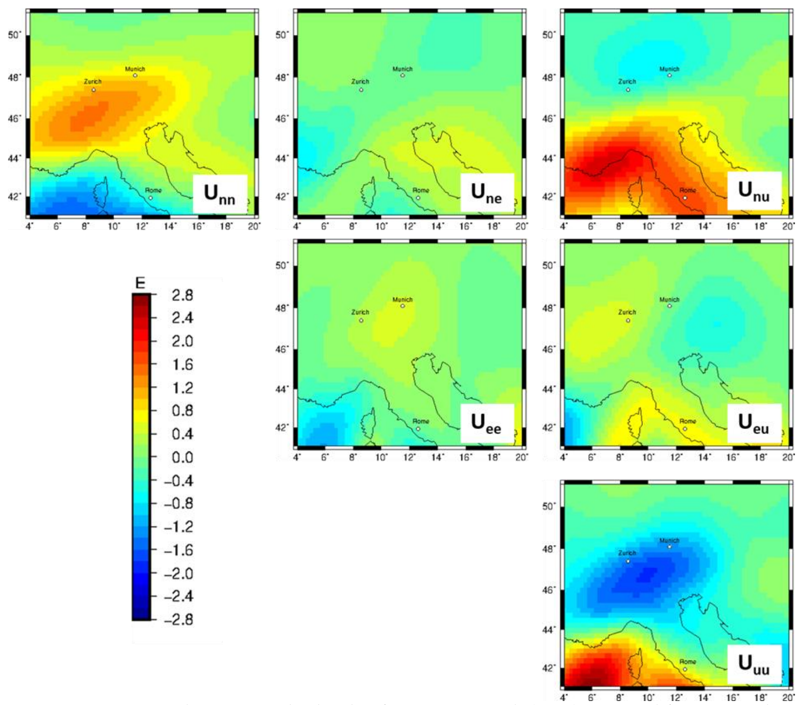

Figure 13 GOCE gradients at 225 km height after Bouman et al. (2016) corrected for topography and bathymetry with a 5° extension to remove far filed effects. The gravity gradients are presented in a North-East-Up coordinate system.

The forward calculated gzz component at 225 km station height from a density model (section 3) with converted densities ranges from -3.5 E to 0.7 E (Fig. 14). A positive gravity signal of about 0.5 E in the Apennine and Alpine region is observed which could be linked to subducting slab segments. However, it is impossible to separate specific slab segments.

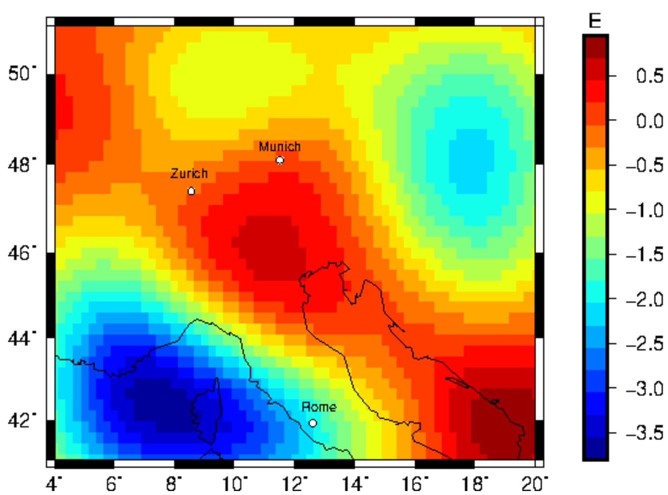

Figure 14 Forward calculated gravity signal from relative density distribution converted from relative seismic velocities using a conversion factor of 0.3.for the) gzz component at 225 km station height.

https://doi.org/10.5194/se-2020-145
Preprint. Discussion started: 16 September 2020

Forward calculated tesseroid models (section 4.1) for slab configuration 1 and 2 with a constant density contrast of 60 kg/m^3 and a constant thickness of 80 km result in a less sharp gravity signal for the gzz component at a station height of 225 km (Fig. 15) compared to the gz component at station height of 6040 m (Fig. 6). The gravity signal for the gzz component is in the range of 0.8 E to 1 E. At satellite altitude the gravity signal is observed as a large area with a positive gravity effect for Configuration 1 and 2. The contribution of the different slab segments to this positive gravity effect is not distinguishable. The only recognizable difference is the size of this positive gravity signal. Configuration 1 shows a smaller anomaly, due to a lower volume of subducting material in the Eastern Alps.

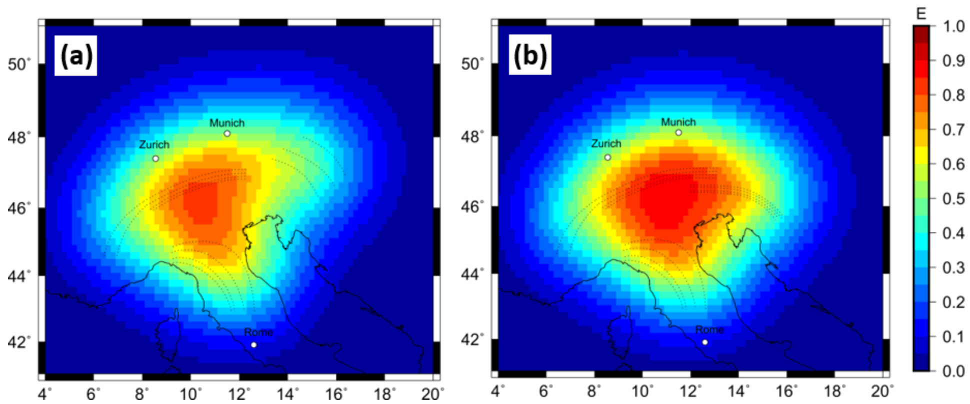

*Figure 15 Forward calculated gzz gravity signal at a station height of 225 km from predefined slab geometries with a content density contrast of 60 kg/ m^3 and a constant thickness of 80 km. **(a)** slab configuration of hypothesis 1 **(b)** slab configuration of hypothesis 2.*

In Addition, the signal strength for the forward calculated gzz component show the same dependency of signal strength to the density contrast and slab thickness (Fig. 16) as the gz component (Fig. 7). The signal strength of the gzz component ranges for the 12 different combinations from 0.3 E to 2 E (Fig. 16). The gravity signal cannot be separated and affiliated to a certain slab segment. The gzz gradient signal shows a large blurry gravity high over the Alps, which thins out to the edges.

https://doi.org/10.5194/se-2020-145
Preprint. Discussion started: 16 September 2020

Solid Earth
Discussions

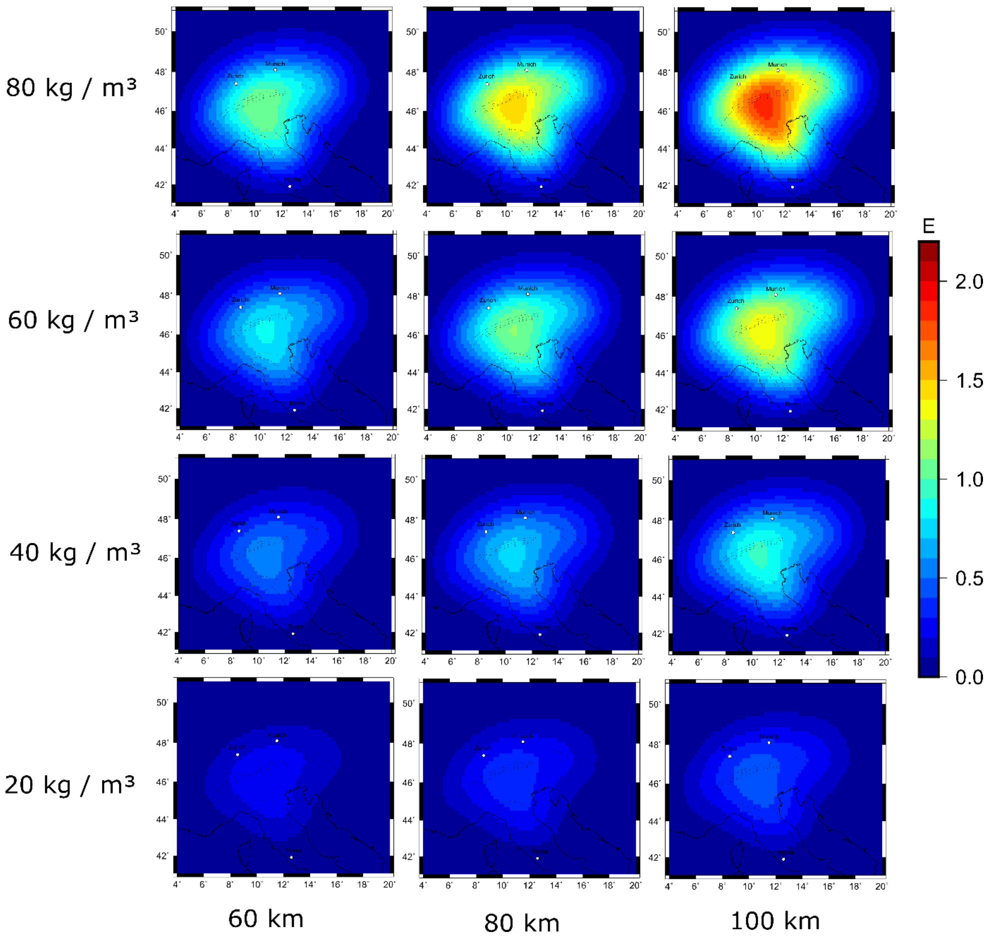

Figure 16 Forward calculated gzz gravity signal for 12 different combination of density contrast and slab thickness at a station height of 225 km for the slab configuration.

The gravity effect for the LitMod models (section 4.2) with the slab Configuration 1 shows in the lithosphere domain a signal strength of about 0.05 E, while the sub lithospheric gravity signal is in the range of 0.1 E for the gzz component at satellite altitude of 225 km height. The combined gravity signal is in the order of 0.14 E (Fig. 17). A Proterozoic slab produces a larger amplitude in signal strength, however the different slab segments can again not be separated (Fig. 18). The purely compositional or thermal effect in the sub lithosphere is comparable to the effect of the gz component (Fig. 12, 18).

https://doi.org/10.5194/se-2020-145
Preprint. Discussion started: 16 September 2020

Solid Earth
Discussions

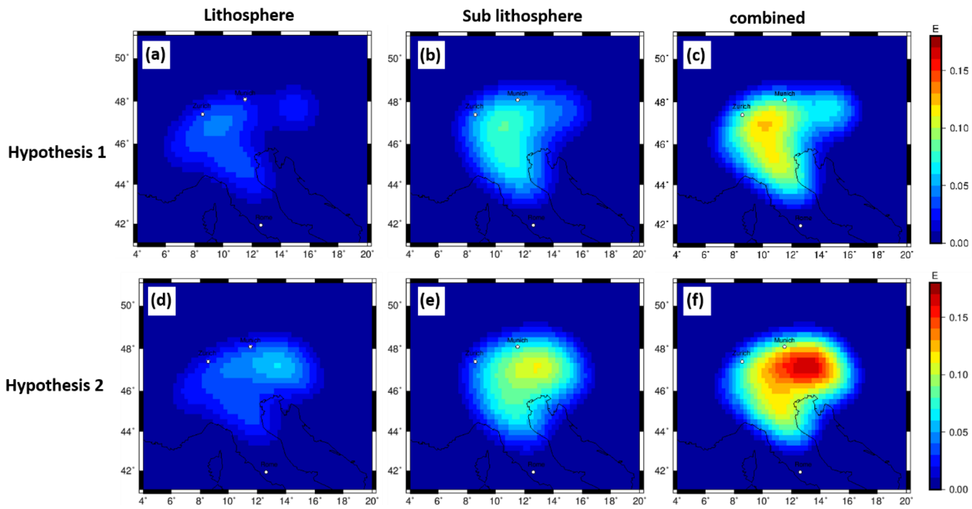

Figure 17 forward calculated gzz gravity signal at satellite altitude of 225 km based on LitMod models with tecton like compositions in the lithosphere and PUM and DMM compositions in the sub lithosphere (M_1, M_2, M_3, M_4) with an additional thermal anomaly of -100° K for the sub-lithospheric slab segment for predefined slab Configuration 1 ***(a)-(c)*** *and for Configuration 2* ***(d)-(f)***.

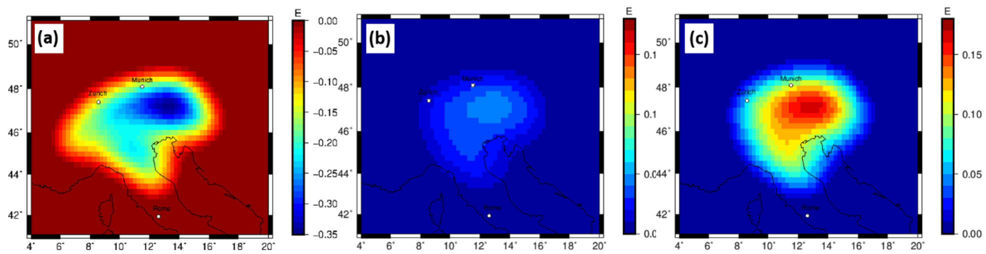

Figure 18 **(a)** Forward calculated gravity effect for the gzz component at satellite height of a Proterozoic lithospheric slab segment to a Tecton compositional ambient mantle for Configuration 2. **(b)** gravity signal produced by purely compositional effect in the sub lithosphere between a PUM and DMM composition. **(c)** gravity signal produced by purely thermal anomaly of -100° K for a sub lithospheric slab segment.